Eur. Phys. J. AP **5**, 127–134 (1999)

THE EUROPEAN PHYSICAL JOURNAL APPLIED PHYSICS

Ultrasonic attenuation spectroscopy and light scattering study of the ageing of very fine emulsions

N. Herrmann[1] and P. Lemaréchal[2,a]

[1] Biopolymers and Colloids Research Laboratory, Department of Food Science, University of Massachusetts, Amherst, MA 01003, USA

[2] Laboratoire de Dynamique des Fluides Complexes, Université Louis Pasteur, 4 rue Blaise Pascal, 67000 Strasbourg, France

Received: 6 August 1998 / Revised: 28 October 1998 / Accepted: 28 October 1998

Abstract. Very fine, 10% vol/vol, *n*-hexadecane and *n*-octadecane oil-in-water emulsions, stabilized by sodium dodecyl sulfate, have been prepared. Due to the very small size of the oil droplets, these emulsions are susceptible to undergo Ostwald ripening and/or coalescence. The maturation of the emulsions was studied over several months by three different techniques: ultrasonic attenuation spectroscopy, static light scattering and dynamic light scattering. Ultrasonic spectroscopy measurements between 0.5 and 10 MHz appeared as the most convenient technique for monitoring the changes in the size of such droplets. Moreover, the correlation of the results from the three different techniques allows a complete determination of the particle size and polydispersity during the ageing.

PACS. 43.35 Bf Ultrasonics, velocity and attenuation in liquids, liquid crystals, suspensions, and emulsions – 82.70 Kj Emulsions and suspensions

1 Introduction

During the last decade, the use of ultrasonic spectroscopy for studying emulsions and suspensions has evolved from laboratory measurements to commercially available particle sizing instruments [1]. Ultrasound can rapidly and non-destructively measure the concentration and the particle size distribution of a dispersion as soon as some of the thermophysical properties of both media are known. The technique has been used to study suspensions [2–4], oil-in-water emulsions [5–8] and water-in-oil emulsions [9,10] at concentrations between 1% and 70% without the need for any sample preparation, even in optically opaque systems. The technique also allows quantitative measurements of crystallization kinetics [11,12] and particle interactions during flocculation [13–16,22] .

The whole set of theories describing the propagation of ultrasound in dispersed media is vast: porous media, dispersions of spherical or cylindrical particles, or of visco-elastic inclusions in visco-elastic matrices have been successfully modelized in the whole frequency domain, including the resonances (see Gaunard and Uberall, Lin and Raptis, Habeger, Schwartz and Margulies).

In this study, we are concerned with the regime in which the size of the inclusions is much smaller than the wavelength of the compressionnal wave. In this case, use can be made of the scattering theories derived by Epstein and Carhart [17], Waterman and Truell [18], Allegra and Halley [19], Lloyd and Berry [20], Ma *et al.* [21]. Previous studies performed on quasi monodisperse emulsions have demonstrated the accuracy of these models [4,7]. An excellent agreement on particle size determination was obtained using three different techniques: ultrasonic attenuation spectroscopy, static light scattering and photon correlation spectroscopy.

For emulsions with particles sizes smaller then 100 nm, the determination of the particle size distribution proves very difficult. In this article, we have used a combination of the three techniques mentioned above to follow the growth of hydrocarbon oil-in-water emulsions whose initial droplet radius was a few tens of nanometers. The discussion of the different results illustrates the possibilities offered by the ultrasonic technique, and the advantage resulting from the association of the different techniques.

2 Materials and methods

2.1 Materials

Emulsions were prepared from *n*-hexadecane, *n*-octadecane and sodium dodecyl sulfate (SDS). All these chemicals were purchased from the Fluka. Chem. Co. and were certified as being at least 99% pure. Double distilled water was used for the preparation of all solutions.

[a] e-mail: plem@ldfc.u-strasbg.fr

2.2 Emulsion preparation

A 36% vol/vol *n*-hexadecane oil-in-water emulsion containing very fine droplets was prepared by homogenizing the oil and a 0.2 M surfactant water solution, using a high-power magnetostrictive device (Vibra Cell 600, Bioblock, Strasbourg, France). During the process, a refrigerated bath was used to prevent heating of the sample. The emulsion was subjected to high power ultrasound until it became transparent and attained the texture of a gel. The particle radius at that time was estimated to be around 30 nanometers.

The same procedure was applied to obtain a 10% vol/vol emulsion of *n*-octadecane in water with 0.051 M SDS in the water phase.

The emulsions were stored at room temperature, the variations never exceeding a few °C, and samples were drawn at regular intervals for analysis. It should be noticed that the freezing point for bulk hexadecane and bulk octadecane are respectively 18.2 and 28.2 °C [11, 12]. However the emulsified droplets undergo supercooling so that their freezing points are respectively around 4 °C and 14 °C, and depend only slightly on the size of the droplets [22].

2.3 Light scattering apparatus

The dependence of the average scattered intensity on the scattering vector q, as well as the apparent diffusion coefficient obtained by first cumulant analysis of the correlation function of the scattered intensity, have both been used for characterizing the size distribution of the droplets. The light scattering experiments have been carried out on a photon correlation spectroscopy apparatus built in the laboratory, using a Spectraphysics 2020 ionized argon laser (λ =488 nm), an EMI-9863 photomultiplier, an amplifier-discriminator and a digital correlator Brookhaven BI8K. The experimental set-up is automated, the scattering angle is controlled by a motorized goniometer and varies between 15° and 140°. The temperature of the cell is regulated and fixed at 20 °C. The samples were studied at an optimum volume fraction of 10^{-5} in order to prevent multiple scattering effects. The dilution was made very carefully so that all samples presented precisely the same oil volume fraction.

2.4 Ultrasonic measurements

All ultrasonic attenuation measurements have been performed with a fixed-path ultrasonic interferometer according to a principle proposed by Eggers [23] and described in a previous paper [7]. The resonator consists of two parallel piezo-electric transducers between which the sample is placed. A programmable frequency synthesizer (Hewlett-Packard 3326 A) delivers a high frequency sinusoidal voltage to the first transducer, which sends an ultrasonic wave in the sample. This wave undergoes multiple reflections inside the cell. The signal detected by the receiving transducer is amplified, digitized by an acquisition card and delivered to a computer.

When the frequency of the exciting signal is varied, the electrical voltage on the receiving transducer shows resonance peaks when the width of the cell corresponds to an integer multiple of half-wavelengths. The width of each resonance peak is then directly related to the ultrasonic attenuation. The computer manages the experiment by controlling the synthesizer in order to find automatically the successive resonances of the cell, and by computing the ultrasonic attenuation at each corresponding frequency. The sample volume needed is about 10 cm^3. The frequency range is 0.5 MHz to 10 MHz, and the precision offered by the technique is around 2% for values of the absorption per wavelength ranging from 10^{-3} to 10^{-1}. All measurements were performed at 25 °C and at 10% oil volume fraction. It has been shown [7] that around this concentration the attenuation is proportional to the concentration, indicating no interactions between the particles. Throughout this article, the losses due to the intrinsic attenuation of each component are subtracted from the result, so that only the excess absorption per wavelength ($\Delta\alpha\lambda$) pertaining to the granular nature of the medium is considered.

3 Results and discussion

The ageing of an *n*-hexadecane oil in-water-emulsion stabilized by SDS has been followed over a period of two months. Samples were drawn periodically from the stock emulsion, and studied by static and dynamic light scattering, and by ultrasonic attenuation spectroscopy.

For analyzing the experimental results, we suppose that the particle size distribution of the emulsion is monomodal; *i.e.* there is only one peak in a plot of droplet concentration *versus* droplet size, which seems a reasonable assumption for the systems that we studied. A mean radius $\bar{r}$, and a polydispersity index σ are then sufficient to describe such a distribution. We assume moreover that the size distribution of the droplets can be properly described by a log-normal distribution $G(r)$ (Eq. (1)) (it has been checked that the use of another monomodal distribution law, such as Schultz law, leads to essentially similar conclusions)

$$G(r) = \frac{1}{\sqrt{2\pi \ln(1+\sigma^2)}} \frac{1}{r} \times \exp\left(-\frac{(\ln(r/\bar{r}) + \ln(1+\sigma^2)/2)^2}{2\ln(1+\sigma^2)}\right) \quad (1)$$

with:

$$\sigma^2 = (\overline{r^2} - \bar{r}^2)/\bar{r}^2. \quad (2)$$

The successive moments of the log-normal distribution are conveniently given by :

$$\overline{r^n} = \int_0^\infty r^n G(r) dr = \bar{r}^n (1+\sigma^2)^{n(n-1)/2}. \quad (3)$$

The contribution of a class of particles to the ultrasonic properties of the suspension is a function of the volume they represent, (and of the square of this volume in the case of light scattering [24]). It is thus appropriate to define the distribution of the particle sizes in terms of their volume distribution $G_3(r)$ (Eq. (4)) and of their volume average radius r_{43}, which can be expressed as a function of the number average radius $\bar{r}$, and of the polydispersity index (Eq. (5)):

$$G_3(r) = r^3 G(r) \tag{4}$$

$$r_{43} = \frac{\int_0^\infty r G_3(r) dr}{\int_0^\infty G_3(r) dr} = \bar{r}(1+\sigma^2)^3. \tag{5}$$

It is interesting to note that the volume distribution function $G_3(r)$ and the number distribution function $G(r)$ possess the same value of the polydispersity index σ. Indeed $G_3(r)$ is "wider" than $G(r)$, but its mean is shifted towards higher values of the radius in the same proportion.

Our purpose is to try to characterize our samples by deducing the size distribution parameters r_{43} and σ from the observed ultrasound and light scattering results.

3.1 Ultrasonic attenuation spectroscopy

The propagation of an ultrasonic wave in an emulsion is now well-understood. In this work, we have made use of an approach based on the work of Epstein and Carhart [17] and of Lloyd and Berry [20]. Since this approach has been reviewed in detail elsewhere [25], we only outline the essential features.

The scattering of an incident plane compression wave by a spherical particle generates three additional waves in each medium: a compression wave, a shear wave and a thermal wave, which propagate inside the particle and in the fluid matrix. The thermal and the shear waves are rapidly attenuated and are responsible for the loss of ultrasonic energy.

In emulsions, which usually present a low density contrast between the two phases, the contribution of the thermal waves is the governing mechanism. The frequency behavior of the ultrasonic properties is then controlled by the time required for the diffusion of heat across the particle, this time is proportional to square of the radius. The excess absorption per wavelength of an emulsion is described by a complicated equation in which the thermal and physical properties of the two phases play a role. The spectra present a maximum that is a function of the volume fraction ϕ_ν and of a reduced variable fr^2 [25], product of the frequency by the square of the radius. Note that this is no longer true at very high frequencies or for very large particles, where the scattering effects become predominant. The use of the above theory is subject to the following additional restrictions, which are satisfied for small particles and moderate concentrations:

– the size of the particles must be much smaller than the compression wavelength in the continuous phase;

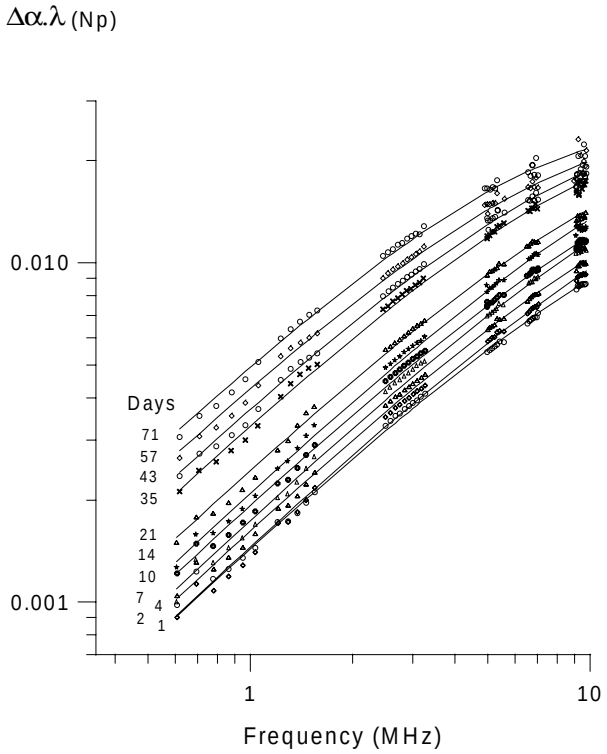

Fig. 1. Evolution of the ultrasonic attenuation spectra during the ageing of a 10% vol/vol n-hexadecane/water emulsion. Curves are best fit to theoretical values. A variation of 1 nm of the apparent radius can easily be distinguished.

– the particles must be randomly distributed, and the distance between the particles has to be larger than the penetration depth of the viscous and thermal waves in the continuous phase.

The position in frequency of the attenuation spectrum varies thus like $1/r^2$, which makes ultrasound very sensitive to size changes. Figure 1 shows the variation of the excess attenuation per wavelength, $\Delta\alpha\lambda$, measured in a 10% n-hexadecane in water emulsion as a function of time. The steady shift of the spectra towards low frequencies clearly indicates an increase of the particle size over time. A variation of 2% of ultrasonic absorption corresponds here to a variation of 1% in the droplet size, and is easily detected.

For each attenuation spectrum the mean radius and the polydispersity index are determined by a least square fit method: these two quantities are the only adjustable parameters, as the total volume fraction of the droplets is known, as well as the values of the relevant thermodynamic constants (*cf.* Tab. 1).

This analysis of the measurements clearly shows an increase of the mean radius r_{43}, seemingly accompanied by a decrease of the polydispersity σ during the two months storage time. It must be observed however that the values obtained for r_{43} are much more reliable than the values obtained for σ: when performing the least-squares procedure it can be observed that the sum of the squares of the residues varies very rapidly when r_{43} is varied, and rather slowly when σ is varied. In fact, for each spectrum,

Table 1. Thermo-physical constant of materials at 25 °C.

	n-hexadecane	n-octadecane	water
Sound velocity c (ms^{-1})	1340 (a)	1361 (c)	1496.7 (d)
Density ρ (kg m^{-3})	769.3 (a)	778.3 (c)	997.1 (b)
Thermal dilatation β (K^{-1})	8.145×10^{-4} (a)	8.69×10^{-4} (c)	2.57×10^{-4} (b)
Shear viscosity η (kg m^{-1} s^{-1})	0.00334 (b)	0.00471 (b)	0.00089 (b)
Specific heat C_p (J kg^{-1} K^{-1})	2217 (b)	2220 (c)	4180 (b)
Therm. cond. κ (W m^{-1} K^{-1})	0.143 (e)	0.153 (f)	0.609 (b)
Sound attenuation α (m^{-1})	$101 \times 10^{-15} f^2$ (a,e)	$116 \times 10^{-15} f^2$ (c)	$23 \times 10^{-15} f^2$ (a)

(a) Measured in the laboratory.
(b) Handbook of chemistry and physics 66th edition.
(c) Extrapolation from measurements.
(d) V.A. Del Grosso, C.W. Mader "Speed of sound in pure water", JASA **52**, 1972.
(e) Epstein and Carhart [17].
(f) R.W. Powel, A.R. Challoner, "Thermal conductivity in N-octadecane" Ind. Eng. Chem. **53**, 581 (1961).

a number of possible couples (r_{43}, σ) can be determined, so that r_{43} can be considered as a function of σ, this function being the locus of the minima of the sum of the squares of the residues.

As can be seen in Figure 2, a remarkable and surprising observation is that, for all spectra, the value obtained for r_{43} is almost independent of the value chosen for σ: the volume average radius r_{43} appears thus as very pertinent for characterizing the size of small droplets.

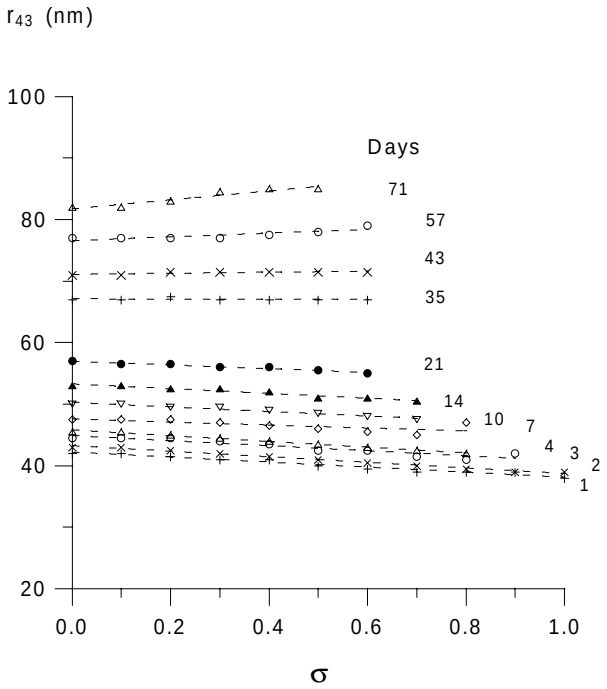

Fig. 2. Combinations of the values of radius and polydispersity (r_{43}, σ) which lead to the best fit for each ultrasonic attenuation spectrum (the dashed lines are guides for the eye). The estimation of the volume average radius r_{43} is fairly insensitive to the polydispersity, which makes it a good parameter for characterizing emulsions.

3.2 Static light scattering

The form factor (normalized angular intensity profile) of an homogeneous spherical particle presents a series of maxima and minima as a function of the scattering vector q and of the radius r. This is the way by which the size of the particle can be deduced from the angular variations of the scattered intensity. If the Rayleigh-Ganz-Debye criterion (particle size much smaller than wavelength) is satisfied, the form factor is given analytically by:

$$P(qr) = \frac{9}{(qr)^6}(\sin(qr) - qr\cos(qr))^2 \qquad (6)$$

where

$$q = \frac{4\pi}{\lambda} n_s \sin(\theta/2). \qquad (7)$$

λ is the wavelength of the incident light, n_s the refractive index of the particle and θ the scattering angle.

If this condition is not fulfilled, the Mie theory must be used to compute the form factor $P(q, r)$. The scattered intensity for a distribution $G(r)$ of particles is then given by [24] :

$$I(q) \propto \int_0^\infty r^6 P(q, r) G(r) dr. \qquad (8)$$

Due to the small size of our emulsions the first minimum of the scattered intensity is out of range of our equipment, and due to the polydispersity the shape of the curve is less marked, so that the analysis of the results is particularly difficult and the particle size determination is less secure, all the more since we have here three adjustable parameters.

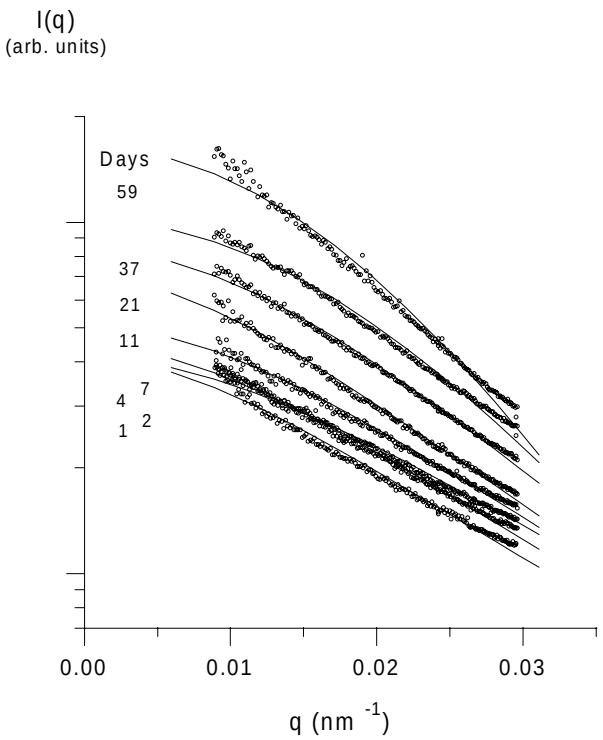

Fig. 3. Evolution of the form factor (light intensity *versus* scattering wave vector) during the ageing of a 10% vol/vol n-hexadecane/water emulsion. Curves are best fit to theoretical values. The large increase of the scattered intensity expresses the growth of the droplets.

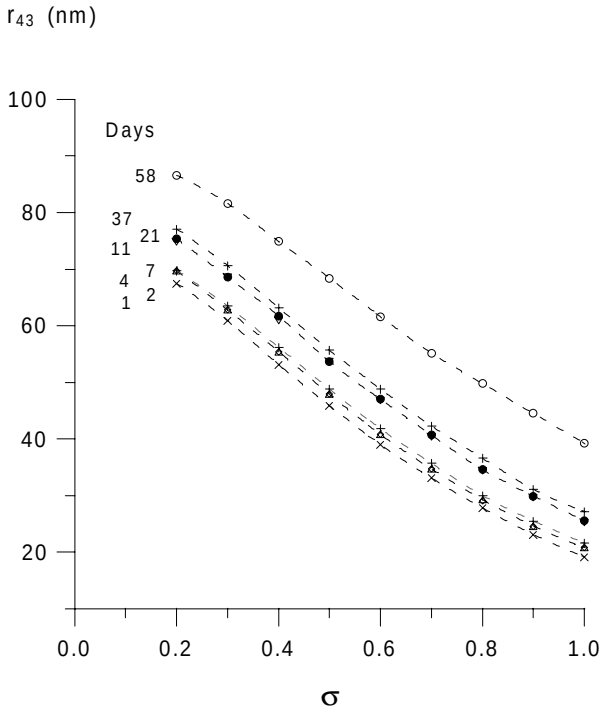

Fig. 4. Combinations of the values of radius and polydispersity (r_{43}, σ) which lead to the best fit for each static light scattering experiment (the dashed lines are guides for the eye). It is virtually impossible here, to ascertain the values of both r_{43} and σ.

The variation with time of the form factor of the emulsion is presented in Figure 3. The same least squares procedure has been used in order to fit the data, the small discrepancy between fit and measurements for the low values of the wave vector can be explained by the imperfections of the geometry of the set-up. At higher angles, the discrepancy is mainly due to the fact that the scattered intensity is very weak and may become comparable to the parasitic light backscattered by the faces of the sample holder.

Her again we determine, for different values of σ, the value of r_{43} (and of an amplitude coefficient) that minimize the sum of the squares of the differences between the measurements and the calculated curve. It was only possible in this case also, to obtain a relation between r_{43} and σ for each experimental curve. The results of this analysis are presented in Figure 4. Contrary to what was observed in the case of ultrasound, the values of the mean radius are here strongly dependent on the polydispersity.

However an additional information can be gained from the fact that all samples have been studied at the same oil volume fraction ϕ_ν. This imposes a relation between the extrapolated intensity at zero q and the parameters of the distribution r_{43} and σ:

$$\lim_{q\to 0} I(q) \propto \phi_\nu \frac{\overline{r^6}}{\overline{r^3}} = \phi_\nu r_{43}^3 (1+\sigma^2)^3. \qquad (9)$$

As a result, the normalized intensity $I(0)/(r_{43}(1+\sigma^2))^3$ must remain constant during the change in size. This result will be used in Section 3.4 of the discussion.

3.3 Dynamic light scattering

Photon Correlation Spectroscopy (PCS) offers a simple and accurate measure of the size over a range of radii varying from 2 nm to several micrometers. However, information about particle size distribution is difficult to obtain in the case of small particles. Cumulant analysis or Laplace transform [26] are insensitive to small polydispersities. A cumulant analysis of our data has led to inconsistent results.

We have applied a method described by Pusey [24], which takes advantage of the q dependence of the apparent diffusion coefficient $D_a(q)$.

The apparent particle diffusion coefficient $D_a(q)$ given by the first cumulant of the scattered light intensity (the initial slope of the logarithm of the autocorrelation function) was measured in function of time at scattering angles between 40 and 100 degrees.

For a monodisperse emulsion the diffusion coefficient is related to the hydrodynamic radius of the particles by Stokes-Einstein relation (12):

$$D(r) = \frac{kT}{6\pi\eta r} \qquad (10)$$

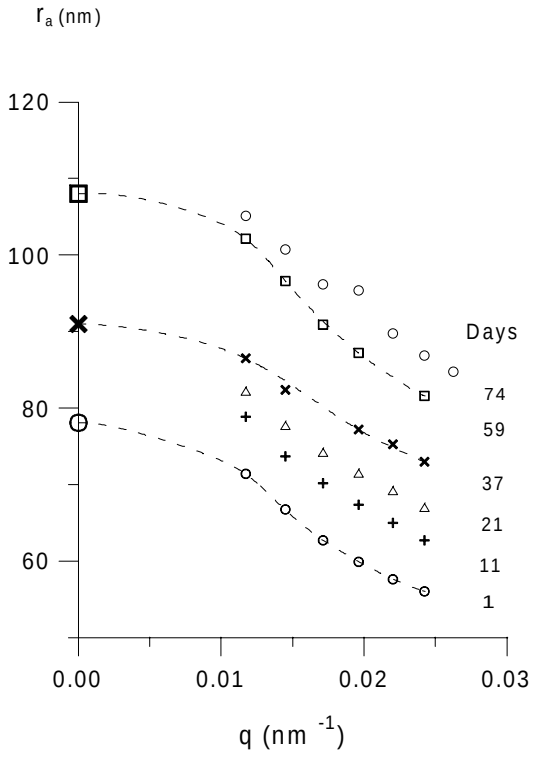

Fig. 5. Evolution with time of the apparent particle radius determined by photon correlation spectroscopy in function of the scattering wave vector. Attempts to fit theoretical curves were unsuccessful. Qualitatively the slope of the curves indicates a noticeable polydispersity, and the increase of the droplet size is clearly visible. The apparent radius at $q = 0$ for 3 different dates, calculated with the values of r_{43} and σ deduced from static light scattering and ultrasound experiments, is also indicated (large symbols).

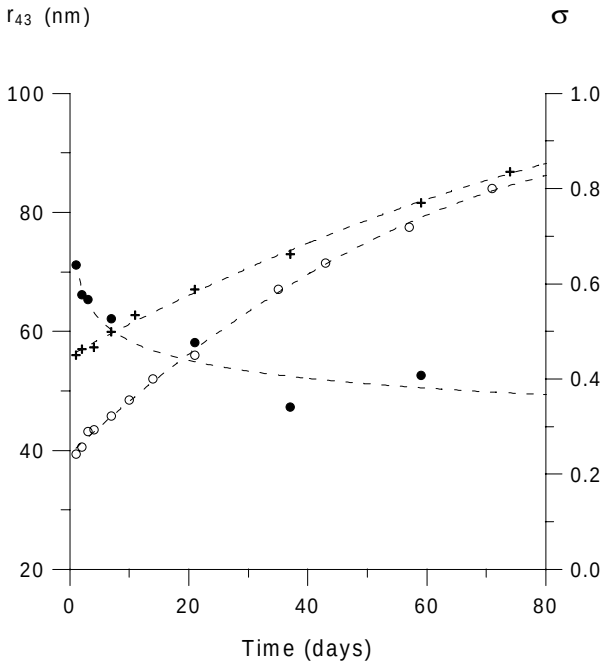

Fig. 6. Variation of the mean radius r_{43} (○) and the polydispersity σ (●) with time during the ageing of the hexadecane in water emulsion. Also plotted is the apparent hydrodynamic radius (+) determined at 90° by dynamic light scattering: the estimations are heavily overestimated for the smallest and most polydisperse emulsions.

where kT is the thermal energy and η the shear viscosity of the continuous phase. In this case $D(r)$ is not dependent on the wave vector q.

For a particle size distribution an apparent diffusion coefficient $D_a(q)$ is measured, from which an apparent radius r_a can be deduced by use of equation (10). This intensity-weighted average coefficient is given by:

$$D_a(q) = \frac{\int_0^\infty r^6 P(qr) D(r) G(r) dr}{I(q)} \cdot \qquad (11)$$

The measurements of r_a are presented in Figure 5 *versus* the scattering wave vector q. The increase with time of the apparent radius is clearly visible, while the angular dependence of r_a shows that the samples are polydisperse. However, it was not possible to obtain a satisfying fit of the experimental results with the above relation, particularly during the beginning of the ageing. The method proposed by Pusey [24] to describe the diffusion in the case of small polydispersities does not seem to be adequate here.

The extrapolation at $q = 0$ of the apparent coefficient can however give a useful relation, which will be used in the last part of the discussion:

$$D_a(0) = \frac{kT}{6\pi\eta\bar{r}(1+\sigma^2)^5} \cdot \qquad (12)$$

The related apparent radius is then given by:

$$r_a(0) = \bar{r}(1+\sigma^2)^5 = r_{43}(1+\sigma^2)^2. \qquad (13)$$

3.4 More accurate determination of the size

We have seen the difficulty, for each of the light scattering techniques that we have used, to characterize completely and accurately the droplet size distribution. This difficulty is related to the particularly small size of the particles studied.

However the ultrasonic and the static light scattering measurements provide two independent relations between r_{43} and σ (Figs. 2 and 4). These relations are simultaneously verified by a unique couple of values of r_{43} and of σ, which can be thus ascertained.

The values of r_{43} and of σ determined by this method are plotted as a function of time in Figure 6. Over the two months period, the size of the droplets increased while the polydispersity clearly decreased. It has been verified that all these (r_{43}, σ) pairs lead to a constant value of the normalized intensity $I(0)/(r_{43}(1+\sigma^2))^3$, which is an important confirmation of the validity of the analysis.

We have reported in Figure 5, for three different times, the values $r_a(0)$ obtained from the diffusion constant extrapolated at $q = 0$ predicted with the above values of r_{43} and σ. The agreement of these points with the experimental results is quite acceptable.

The apparent radius deduced from the diffusion constant measured at 90° has also been plotted in Figure 6. This value is often used in common practice as a reference for droplet size characterization. Our data clearly show that this value leads to a significant overestimation of the size, especially for large polydispersities.

The same procedure has been used to follow, during more than six months, the growth of droplets for an *n*-octadecane oil-in-water emulsion. During this period the radius r_{43} of the emulsions determined by ultrasound increased from 28 nm to 43 nm.

3.5 Discussion of the results

As shown by Kabalnov *et al.* [27], owing to the small size of the droplets and to the high concentration of surfactant, the ageing process is essentially due to Ostwald ripening, that is to the mass transport of oil from small droplets to large droplets through diffusion of oil molecules in water. This phenomenon is described by the theory of Lifshitz-Slezov-Wagner and its subsequent modifications, see for instance the review article of Voorhees [28].

The theory predicts that, after a transient regime, the system tends towards an asymptotic state independent of the initial conditions. In this regime the cube of the average radius increases linearly with time, and the distribution of the particle radii is given by a unique function of the reduced variable $r/\bar{r}$, ratio of the radius to the average radius. Therefore the relative width of the size distribution tends towards a constant value, and an initially wide size distribution will narrow with time. From data in reference [28] this limit of the relative width of the distribution can be estimated to be around 0.20 for the LSW theory, or above 0.25 for more recent theories which take into account the Brownian motion of the droplets and the effect of particles interactions on the diffusion field.

The results presented in Figure 6 are virtually in quantitative agreement with the values above as regards the width of the distribution for long times.

Figure 7 presents the variation, as a function of time, of the cube of r_{43}, *i.e.* of the mean volume of the droplets, for the hexadecane and the octadecane emulsions. The observed linear time dependence of the volume of the droplets is in direct agreement with the predictions of the theory. The slopes of the two lines lead to an estimation of the ripening rates close to 0.11 $\mathrm{nm^3 s^{-1}}$ and 0.0045 $\mathrm{nm^3 s^{-1}}$ for the hexadecane and the octadecane emulsions respectively.

It is interesting to compare these values to the results of the extensive study performed by Kabalnov *et al.* [27] on a series of hydrocarbons emulsions (*n*-nonane to *n*-hexadecane). Kabalnov reports a value of 0.087 $\mathrm{nm^3 s^{-1}}$ for the ripening rate of the hexadecane emulsion. An estimation of the ripening rate for the octadecane can be deduced by extrapolation of the results obtained on the whole set of hydrocarbons, which appear to follow very tightly a geometric progression: due to the decreasing solubility of the oil molecules, the ripening rate decreases as the chain length increases. The ripening rate for octadecane could in this manner be estimated around 0.0060 $\mathrm{nm^3 s^{-1}}$.

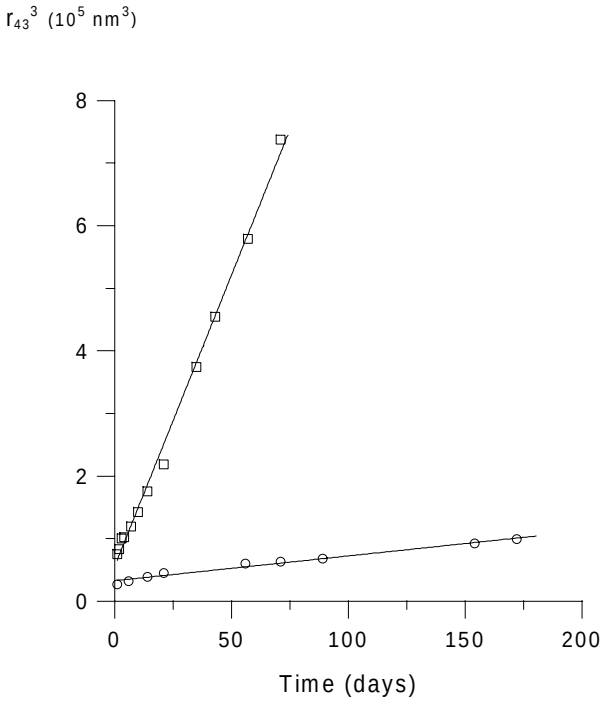

Fig. 7. Variation along time of the mean droplet volume determined by ultrasonic spectroscopy for hexadecane (○) and octadecane (□) emulsions. The theory describing Ostwald ripening predicts the observed linear dependence. The growth of the octadecane emulsion is much slower, this can be attributed to the lower solubility in water of the octadecane molecule and also to the lower oil concentration of the stock emulsion (ϕ_ν was 0.36 for hexadecane and 0.1 for octadecane).

Our observations appear thus to be very consistent with the results of Kabalnov. It must be observed however, that we express the ripening rate as the cube of r_{43}, which is certainly somewhat greater than the cube of $\bar{r}$. Besides the oil fraction of our hexadecane emulsion was 0.36 compared to 0.1 for the study of Kabalnov, so that the comparison is to be made with some caution.

4 Conclusion

Static and dynamic light scattering as well as ultrasonic attenuation measurements have been performed on emulsions containing small droplets, in order to monitor the growth due to Ostwald ripening, and possibly to coalescence. The light scattering results, taken alone, were unable to supply an acceptable estimation of the size and polydispersity of the emulsions, while ultrasonic spectroscopy lead to a very reliable estimation of the volume

average radius of the droplets, and, with a lesser degree of accuracy, of the width of their size distribution.

By combining the data from ultrasound spectroscopy and from static light scattering it becomes possible to get a complete characterization of the emulsions, both in size and in polydispersity. The common practice fixed 90° angle photon correlation spectroscopy is shown to be inaccurate in the case of emulsions containing very small droplets with a wide size distribution.

Our results have shown a linear increase of particle volume over time and an associated decrease of the width of the initial particle size distribution, which are both predicted by the theories of Ostwald ripening, and whose numerical values can be accounted for by the theoretical models with a very satisfying accuracy.

Ultrasonic attenuation spectroscopy in the Megahertz range appears thus as a precise and convenient tool for measuring particles sizes as small as a few tens of nanometers.

The authors are very grateful towards Professor D.J. McClements for advice, and towards Professor J.P. Munch for fruitful discussion and help during light scattering experiments. This work has been supported by L'Oréal Company and by the Cooperative State Research, Education and Extension Service, U.S. Department of Agriculture (under Agreement Number 97-35503-4371).

References

1. M.J.W. Povey, *Ultrasonic techniques for fluids characterisation* (Academic Press, 1997).
2. A.K. Holmes, R.E. Challis, D.J. Wedlock, J. Colloid Interface Sci. **68**, 339 (1994).
3. A.S. Dukhin, P. Goetz, Langmuir **12**, 4987 (1996).
4. U. Kaatze, C. Trachimov, R. Pottel, M. Brai, Ann. Phys. **5**, 13 (1996).
5. D.J. McClements, J. Acoust. Soc. Am. **91**, 849 (1992).
6. A. Schroder, E. Raphael, Eur. Phys. Lett. **17**, 565 (1992).
7. N. Herrmann, P. Boltenhagen, P. Lemaréchal, J. Phys. II France **6**, 1389 (1996).
8. Y. Hemar, N. Herrmann, P. Lemaréchal, R. Hocquart, F. Lequeux, J. Phys. II France **7**, 637 (1997).
9. Æ. Nesse, K.-E. Fræysa, IEEE Utrasonic Sympos. Proc. **1**, 499 (1996).
10. P. Aurenty, A. Schroder, A. Gandini, Langmuir **11**, 4712 (1995).
11. E. Dickinson, D.J. McClements, M.J.W. Povey, J. Coll. Interface Sci. **142**, 103 (1991).
12. E. Dickinson, J. Ma, M.J.W. Povey, J. Chem. Soc. Faraday Trans. **92**, 1213 (1996).
13. D.J. McClements, J. Colloid. Interf. Sci. **142**, 103 (1991).
14. N. Herrmann, Y. Hemar, P. Lemaréchal, D.J. McClements (submitted).
15. D.J. McClements, Coll. Surf. A: Phys. Ing. Asp. **90**, 25 (1994).
16. T.K. Basaran, K. Demetriades, D.J. McClements, Coll. Surf. A: Phys. Ing. Asp. **136**, 169 (1998).
17. P.S. Epstein, R.R. Carhart, J. Acoust. Soc. Am. **25**, 553 (1953).
18. P.C. Waterman, R. Truell, J. Acoust. Soc. Am. **2**, 512 (1961).
19. J.R. Allegra, S.A. Hawley, J. Acoust. Soc. Am. **51**, 1545 (1972).
20. P. Lloyd, M.V. Berry, Proc. Phys. Soc. **91**, 678 (1967).
21. Y. Ma, V.K. Varadan, V.V. Varadan, J. Acoust. Soc. Am. **87**, 2779 (1990).
22. N. Herrmann, Ph.D. thesis, University Louis Pasteur, Strasbourg, France, 1997.
23. F. Eggers, Th. Funck, Rev. Sci. Instrum. **44**, 969 (1973).
24. P.N. Pusey, W. van Megen, J. Chem. Phys. **80**, 3513 (1984).
25. D.J. McClements, M.J.W. Povey, J. Phys. D: Appl. Phys. **22**, 38 (1989).
26. H.Z. Cummins, E.R. Pike, *Photon correlation and light beating spectroscopy* (Plenum, New York, 1974).
27. A.S. Kabalnov, K.N. Makarov, A.V. Pertzov, E.D. Schukin, J. Coll. Interf. Sci. **138**, 98 (1990).
28. P.W. Voorhees, J. Stat. Phys. **38**, 231 (1985).